

Measurement of the $1f_{7/2}$ -Neutron-Orbit Radius in ^{41}Ca

S. Platchkov,⁽¹⁾ A. Amroun,⁽¹⁾ P. Bricault,⁽¹⁾ J. M. Cavedon,⁽¹⁾ P. K. A. de Witt Huberts,⁽²⁾ P. Dreux,⁽¹⁾
 B. Frois,⁽¹⁾ C. D. Goodman,⁽³⁾ D. Goutte,⁽¹⁾ J. Martino,⁽¹⁾ V. Meot,⁽¹⁾ G. A. Peterson,⁽⁴⁾ X. H. Phan,⁽¹⁾
 S. Raman,⁽⁵⁾ and I. Sick⁽⁶⁾

⁽¹⁾*Département de Physique Nucléaire, Centre d'Etudes Nucléaires de Saclay, F-91191 Gif-sur-Yvette, France*

⁽²⁾*NIKHEF-K, 1009 AJ Amsterdam, The Netherlands*

⁽³⁾*Indiana University Cyclotron Facility, Bloomington, Indiana 47401*

⁽⁴⁾*University of Massachusetts, Amherst, Massachusetts 01003*

⁽⁵⁾*Oak Ridge National Laboratory, Oak Ridge, Tennessee 37830*

⁽⁶⁾*Department of Physics, University of Basel, CH 4056, Basel, Switzerland*

(Received 7 June 1988)

The magnetic form factor of ^{41}Ca has been measured by elastic electron scattering in the momentum-transfer range between 1.8 and 3.3 fm^{-1} . The $1f_{7/2}$ -neutron-orbit radius inferred from these data definitely demonstrates that the explanation of the Coulomb-energy anomaly cannot be found in a reduction of the valence-orbit radius.

PACS numbers: 25.30.Bf, 21.10.Sf, 27.40.+z

Precise measurements of nuclear radii serve as benchmarks for microscopic descriptions of nuclei. Mean-field calculations offer one of the best methods for describing nuclear ground-state properties. Their predictions are in excellent agreement with experimental charge radii determined from elastic electron scattering and muonic-x-ray energies. However, theoretical valence-nucleon radii are significantly larger than those deduced from binding-energy differences between mirror nuclei with the same doubly closed-shell core. Analyses¹ of these Coulomb-energy differences (CED's) have led to valence radii that are 10% to 20% smaller than the mean-field predictions. Numerous corrections to the shell model have been calculated,²⁻⁵ but without significant improvement in the valence-radii comparison. ^{41}Ca is the generic example for the CED anomaly. Mean-field calculations predict its $1f_{7/2}$ -valence-neutron radius to lie in the range 4.0–4.2 fm (Refs. 6 and 7), while the CED's for the ^{41}Ca - ^{41}Sc pair would be consistent¹⁻⁵ with a range of 3.6–3.8 fm. Precise measurement of its valence-nucleon radius is therefore of particular value.

Magnetic elastic electron scattering^{8,9} offers an elegant technique for measurement of the valence radius. For a nucleus with a doubly closed core and a valence nucleon in a stretched configuration ($j = l + \frac{1}{2}$) the interpretation is particularly simple: The shape of the highest magnetic multipole is given by the Fourier-Bessel transform of the radial wave function of the valence nucleon. This technique has been used¹⁰ to determine the radius of the $1f_{7/2}$ orbit for the valence protons in ^{51}V and for the valence neutrons in ^{49}Ti , but the corresponding cores are not doubly closed. With a single $1f_{7/2}$ nucleon outside a doubly closed ^{40}Ca core, ^{41}Ca is an ideal case for a measurement of the $1f_{7/2}$ -neutron-orbit radius. Measurements on ^{41}Ca were not possible in the past, because the ^{41}Ca isotope is unstable ($T_{1/2} = 10^5$ y) and was

only available in very small quantities. Through neutron irradiation of ^{40}Ca at the Oak Ridge High-Flux Isotope Reactor and subsequent mass separation, a ^{41}Ca target of thickness suitable for an electron scattering experiment was produced. In this Letter we report on the first measurement of the magnetic form factor of ^{41}Ca via elastic electron scattering.

The experiment was performed at the Saclay linear electron accelerator. As a target we used an enriched calcium carbonate ($^{41}\text{CaCO}_3$) tablet of 7 mm diam that was contained between two thin aluminum foils. The total target thickness was 33.7 mg/cm^2 , corresponding to a Ca thickness of 13.7 mg/cm^2 . The ^{41}Ca isotopic purity was 81.7%. Because of the small dimensions of the target, the beam position was stabilized with a split-foil secondary-emission monitor coupled with a feedback system to two steering coils. To avoid damage to the fragile target, the beam current was limited to 6 μA . The scattered electrons were analyzed with the 900-MeV/c magnetic spectrometer and identified with its detection system.¹¹ Cross sections were measured at 155° for nine incident energies ranging from 175 to 320 MeV. In order to determine the absolute normalization, ^{40}Ca , ^{41}Ca , and ^{12}C data were taken at forward angles for each energy. The ^{41}Ca charge scattering cross section was also measured at 500 MeV up to a momentum transfer $q = 2.3 \text{ fm}^{-1}$. The energy resolution achieved, 50 keV (FWHM), was sufficient to separate the ^{41}Ca peak from the ^{27}Al , ^{16}O , and ^{12}C peaks, even for the smallest recoil energy difference. Figure 1 shows a typical experimental spectrum.

The radiative corrections were unfolded from the experimental spectra by a standard line-shape-fitting technique. Elastic cross sections were extracted for all nuclei present in the calcium-carbonate target. The absolute normalization of the data was determined to $\pm 3\%$ from

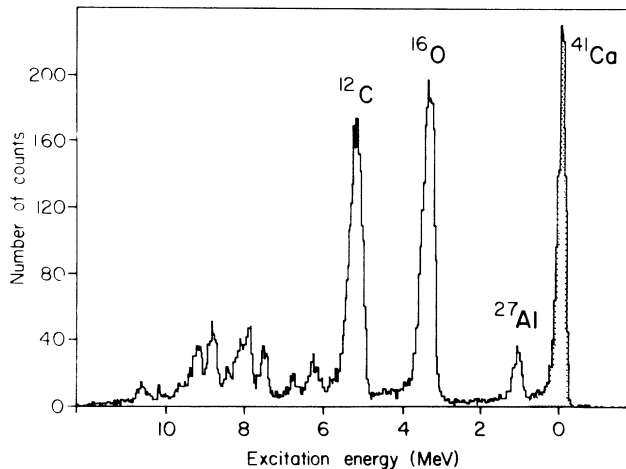


FIG. 1. Experimental (e, e') spectrum from the $^{41}\text{CaCO}_3$ target at 275 MeV and 52° .

the comparison with the earlier measurements¹² on ^{12}C , ^{16}O , and ^{40}Ca . The experimental forward-angle $^{41}\text{Ca}/^{40}\text{Ca}$ ratios (below 1.3 fm^{-1}) were found to be in good agreement with the ratios predicted by the mean-field calculation of Ref. 7. The magnetic part of the cross section was obtained by subtraction of the charge contribution, measured at 500 MeV and at the same momentum transfer q . Beyond $q = 2.3 \text{ fm}^{-1}$, where no charge measurements on ^{41}Ca were made, the well known ^{40}Ca data¹³ were used instead. In this region the ^{40}Ca and ^{41}Ca angular distributions have no diffraction minima; the corresponding theoretical charge cross sections⁷ differ by less than 10%. For safety we assumed a 20% error for the subtraction in this region; this corresponds to an uncertainty of 4% or less for the magnetic part of the cross sections. The Coulomb distortion of the incoming and outgoing waves was unfolded by use of the code HADES.¹⁴ The final magnetic cross sections and form factors are listed in Table I.

The experimental ^{41}Ca magnetic form factor is shown in Fig. 2 together with the results of three theoretical predictions for the $M7$ multipole. The dash-dotted and the solid curves correspond to the mean-field predictions of Negele⁶ and Dechargé and Gogny,⁷ respectively. The dotted curve represents a calculation of Kim¹⁵ performed in the framework of the relativistic mean-field approach of Serot and Walecka.¹⁶ The prediction of Ref. 7 is in very good agreement with the experiment. The calculation of Ref. 15 deviates slightly from the data, while the $M7$ form factor of Ref. 6 decreases too rapidly. Its steeper falloff in q space results from a larger extent of the corresponding $1f_{7/2}$ wave function in r space. The dashed curve depicts the result of Ref. 7 when all lower multipoles are also taken into account. Beyond $q = 2 \text{ fm}^{-1}$, these multipoles do not play a significant role. In contrast, because of the large contribution of the predicted $M5$ multipole, the total form factor overestimates the

TABLE I. Experimental results for the 155° elastic electron scattering. Magnetic cross sections and form factors are listed as a function of the momentum-transfer values q . (Coulomb-distortion effects have been unfolded.) The relative uncertainties quoted include a normalization error of $\pm 3\%$, and refer to both cross sections and form factors.

Energy (MeV)	q (fm^{-1})	$d\sigma/d\Omega$ (mb/sr)	$F^2(q)$	Error (%)
175	1.790	4.14×10^{-7}	1.81×10^{-4}	12.7
190	1.937	3.76×10^{-7}	1.94×10^{-4}	9.8
205	2.087	3.42×10^{-7}	2.05×10^{-4}	9.8
220	2.241	2.18×10^{-7}	1.50×10^{-4}	10.0
235	2.392	1.29×10^{-7}	1.01×10^{-4}	11.9
255	2.590	5.98×10^{-8}	5.55×10^{-5}	19.8
275	2.798	2.30×10^{-8}	2.48×10^{-5}	37.1
300	3.055	2.64×10^{-9}	3.39×10^{-6}	32.4
320	3.252	1.76×10^{-9}	2.57×10^{-6}	58.3

data by a large amount below $q = 2 \text{ fm}^{-1}$.

An experimental radius of the $1f_{7/2}$ orbit can be inferred from these data in the framework of the shell model. Data were fitted with a Woods-Saxon radial wave function following the procedure described in Ref. 10. The diffuseness parameter was fixed to $a = 0.60 \text{ fm}$, and the depth of the potential was adjusted to reproduce the experimental $1f_{7/2}$ separation energy. The amplitudes of the $M5$ and $M7$ multipoles and the radius of

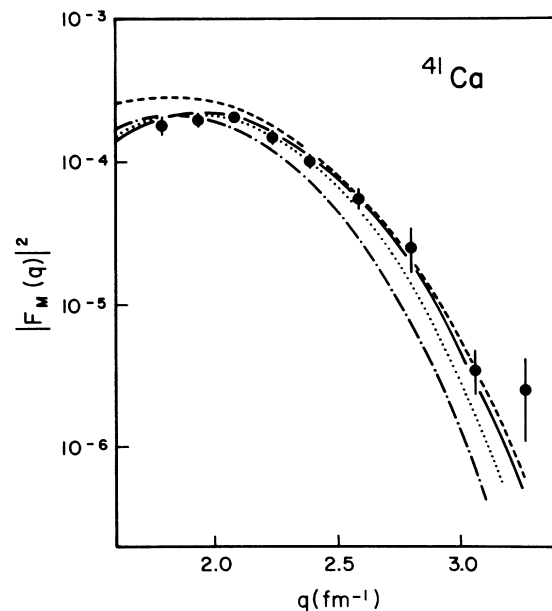


FIG. 2. Magnetic form factor as a function of the momentum transfer q . The data are compared to three theoretical predictions for the $M7$ multipole. The curves depict the mean-field calculations of Ref. 6 (dash-dotted), Ref. 7 (solid), and Ref. 15 (dotted). The dashed curve shows the total form factor (all multipoles included) as calculated in Ref. 7.

the Woods-Saxon potential were fitted to the data. The resulting form factor is shown in Fig. 3. The fit determines the $1f_{7/2}$ neutron radius and the $M7$ amplitude with a statistical error of 1% and 4%, respectively. The $M5$ amplitude has negligible contribution. The $M7$ multipole is thus dominant in the entire momentum-transfer region covered by our experiment and particularly between 1.7 and 2.0 fm^{-1} , where a large contribution from the $M5$ component could also be expected. The comparison with Fig. 2 shows that the observed quenching of the $M5$ multipole is not predicted by theoretical calculations.

The theoretical calculations shown in Fig. 2 do not include meson exchange currents (MEC's) and core-polarization effects.¹⁷⁻¹⁹ Subtracting from the experimental points the MEC contribution as calculated in Ref. 19 and refitting the resulting form factor leads to an increase of the $1f_{7/2}$ radius by 0.8%. An almost identical result is found with the calculation of Ref. 18. The core-polarization effect as calculated in Ref. 19 leads to a 0.2% decrease of the radius. Our fit results, both with and without MEC correction,¹⁹ are given in Table II. These results have a weak model dependence related to the choice of the diffuseness parameter a ; variation of a

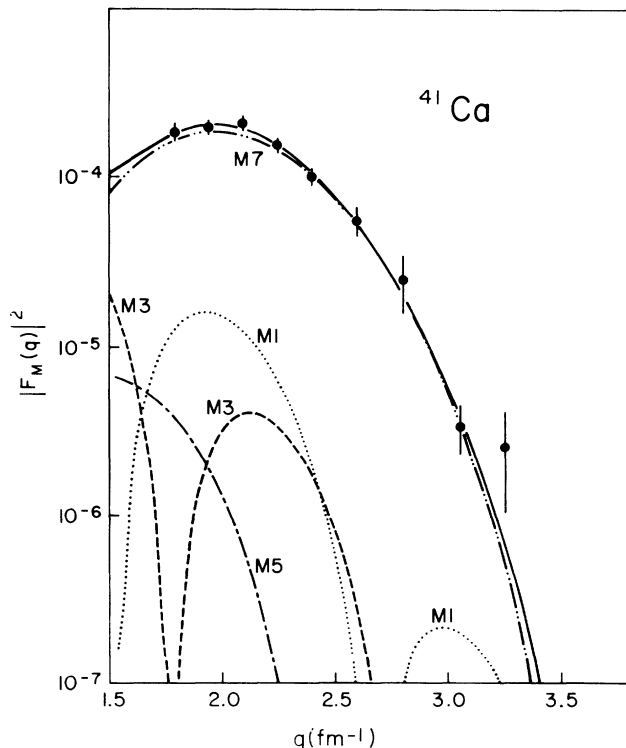


FIG. 3. Best fit to the data (uncorrected for MEC) using a Woods-Saxon wave function. The multipoles shown are $M1$ (dotted), $M3$ (dashed), $M5$ (dash-dotted), and $M7$ (dash-double-dotted). The $M1$ and $M3$ multipoles were calculated with the assumption of a pure single-particle shell model. The solid line depicts the sum of all multipoles.

by ± 0.05 fm results in a modification of the rms radius of $\pm 0.6\%$. The contribution of lower multipoles has negligible effect. The errors quoted include the above model dependence as well as experimental uncertainties. The two essential results deduced from the experiment are the following: (i) The value of the rms radius of the $1f_{7/2}$ neutron orbit is 3.99 ± 0.06 fm; (ii) the single-particle probability a_7 is $(83 \pm 5)\%$, representing a depletion of the $1f_{7/2}$ orbit by $(17 \pm 5)\%$.

The $f_{7/2}$ neutron radius was previously inferred from sub-Coulomb transfer reactions.^{20,21} The values found, 4.00 ± 0.06 fm (Ref. 20) and 3.89 ± 0.12 fm (Ref. 21), are in good agreement with the rms radius found in the present work. Our rms radius also agrees with the mean-field value of 4.02 fm of Ref. 7 and with the relativistic mean-field result¹⁵ of 4.05 fm; it is slightly smaller than the 4.14-fm value of Ref. 4. These observations are consistent with the results obtained for other valence-shell radii¹⁰ available from magnetic electron scattering. In this context it is interesting to note that the $1f_{7/2}$ neutron radius increases by 0.05 fm in going from ^{41}Ca to ^{49}Ti (from must one neutron to seven neutrons in the $f_{7/2}$ shell), in excellent agreement with the mean-field predictions of 0.07 and 0.05 fm from Refs. 6 and 7.

This measurement of the $1f_{7/2}$ neutron radius has direct implications for the interpretation of the Coulomb-energy differences for the ^{41}Ca - ^{41}Sc mirror pair. Indeed, there is a nearly linear dependence² between the value of the valence-orbit radius and the CED. Using the new experimental value for the rms radius and the results of Nolen and Schiffer,¹ we obtain a CED of 6.950(35) MeV. The comparison with the experimental CED value (7.280 MeV) shows a discrepancy of 320(35) keV. Following the approach of Negele,⁴ in which a set of additional corrections was included, the measured radius results in a discrepancy of 450 keV between the experimental and the calculated CED. A comparable range of values, 260–430 keV, is obtained with the more recent results of Auerbach, Bernard, and Van Giai.⁵ Our experiment thus demonstrates that the explanation of the CED anomaly cannot be found in a reduction of the valence-orbit radius.

In conclusion, we have measured the ^{41}Ca magnetic form factor and used the data to determine the radial extent of the $1f_{7/2}$ neutron wave function. The resulting

TABLE II. Experimental values for the rms radius and the spectroscopic amplitude of the $1f_{7/2}$ neutron orbit.

	rms radius (fm)	a_7
Without MEC corrections	3.95 ± 0.06	0.92 ± 0.05
With MEC corrections ^a	3.99 ± 0.06	0.83 ± 0.05

^aReference 19.

rms radius agrees with those predicted by mean-field calculations. Knowledge of this radius definitively removes a fundamental uncertainty for the interpretation of CED anomaly in the $1f_{7/2}$ shell.

This research was sponsored in part by the U.S. Department of Energy under contract with Marietta Energy Systems, Inc. (Oak Ridge). We would like to thank J. Dechargé, M. Girod, E. J. Kim, and J. W. Negele for providing us with their mean-field wave functions. We are also grateful to B. Desplanques and J. W. Negele for fruitful discussions.

¹J. A. Nolen, Jr., and J. P. Schiffer, *Annu. Rev. Nucl. Sci.* **19**, 471 (1968).

²S. Shlomo, *Rep. Prog. Phys.* **41**, 957 (1978).

³Nguyen Van Giai, D. Vautherin, M. Veneroni, and D. M. Brink, *Phys. Lett.* **35B**, 135 (1971).

⁴J. W. Negele, *Nucl. Phys.* **A165**, 305 (1971).

⁵N. Auerbach, V. Bernard, and N. Van Giai, *Phys. Rev. C* **21**, 744 (1980).

⁶J. W. Negele and D. Vautherin, *Phys. Rev. C* **5**, 1472 (1972); J. W. Negele, private communication. For the rms valence-radii comparison, we use the value given in Ref. 4.

⁷J. Dechargé and D. Gogny, *Phys. Rev. C* **21**, 1568 (1980).

⁸T. W. Donnelly and J. D. Walecka, *Nucl. Phys.* **A201**, 81

(1973).

⁹T. W. Donnelly and I. Sick, *Rev. Mod. Phys.* **56**, 461 (1984).

¹⁰S. K. Platchkov, J. B. Bellicard, J. M. Cavedon, B. Frois, D. Goutte, M. Huet, P. Leconte, X. H. Phan, P. K. A. de Witt Huberts, L. Lapikàs, and I. Sick, *Phys. Rev. C* **25**, 2318 (1982).

¹¹P. Leconte *et al.*, *Nucl. Instrum. Methods* **169**, 401 (1980).

¹²H. de Vries, C. W. de Jager, and C. de Vries, *At. Data Nucl. Data Tables* **36**, 495 (1987).

¹³I. Sick, J. B. Bellicard, J. M. Cavedon, B. Frois, M. Huet, P. Leconte, X. H. Phan, and S. Platchkov, *Phys. Lett.* **88B**, 245 (1979).

¹⁴H. G. Andresen, M. Engel, M. Muller, and H. J. Ohlbach, *Nucl. Phys.* **A358**, 365c (1981).

¹⁵E. J. Kim, Ph.D. thesis, Stanford University, 1987 (unpublished), and private communication.

¹⁶B. D. Serot and J. D. Walecka, *Adv. Nucl. Phys.* **16**, 1 (1986).

¹⁷J. Dubach, *Nucl. Phys.* **A340**, 271 (1980).

¹⁸J. F. Mathiot and B. Desplanques, *Phys. Lett.* **101B**, 141 (1981).

¹⁹T. Suzuki, H. Hyuga, and A. Arima, *Z. Phys. A* **293**, 5 (1979); T. Suzuki, Ph.D. thesis, University of Tokyo, 1978 (unpublished).

²⁰G. D. Jones, J. L. Durell, J. S. Lilley, and W. R. Phillips, *Nucl. Phys.* **A230**, 173 (1974).

²¹J. L. Durell, C. A. Harter, J. N. Mo, and W. R. Phillips, *Nucl. Phys.* **A334**, 144 (1980).

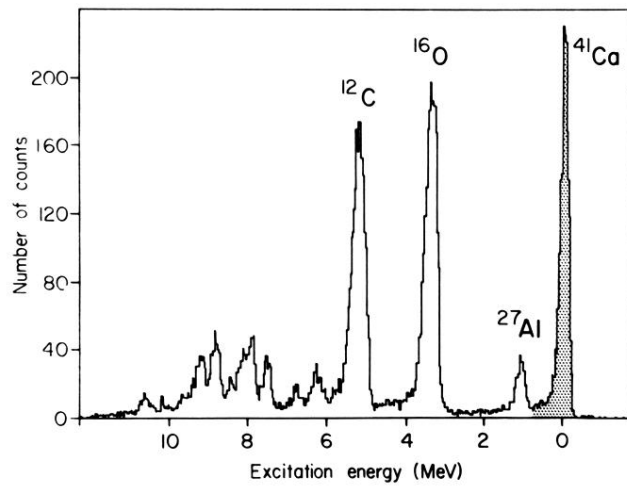


FIG. 1. Experimental (e, e') spectrum from the $^{41}\text{CaCO}_3$ target at 275 MeV and 52° .